THE JOURNAL OF PHYSICAL CHEMISTRY LETTERS
A JOURNAL OF THE AMERICAN CHEMICAL SOCIETY

pubs.acs.org/JPCL

Letter

Melting Curve of Black Phosphorus: Evidence for a Solid−Liquid−Liquid Triple Point

Hermann Muhammad, Mohamed Mezouar,* Gaston Garbarino, Laura Henry, Tomasz Poręba, Max Gerin, Matteo Ceppatelli, Manuel Serrano-Ruiz, Maurizio Peruzzini, and Frédéric Datchi*

Cite This: J. Phys. Chem. Lett. 2024, 15, 8402−8409

Read Online

ACCESS | Metrics & More | Article Recommendations | Supporting Information

ABSTRACT: Black phosphorus (bP) is a crystalline material that can be seen as an ordered stacking of two-dimensional layers, which results in outstanding anisotropic physical properties. The knowledge of its pressure (P)−temperature (T) phase diagram, and in particular, of its melting curve is fundamental for a better understanding of the synthesis and stability conditions of this element. Despite the numerous studies devoted to this subject, significant uncertainties remain regarding the determination of the position and slope of its melting curve. Here we measured the melting curve of bP in an extended P, T region from 0.10(3) to 5.05(40) GPa and from 914(25) to 1788(70) K, using in situ high-pressure and high-temperature synchrotron X-ray diffraction. We employed an original metrology based on the anisotropic thermoelastic properties of bP to accurately determine P and T. We observed a monotonic increase of the melting temperature with pressure and the existence of two distinct linear regimes below and above 1.35(15) GPa, with respective slopes of 348 ± 21 and of 105 ± 12 K·GPa^{-1}. These correspond to the melting of bP toward the low-density liquid and the high-density liquid, respectively. The triple point at which solid bP and the two liquids meet is located at 1.35(15) GPa and 1350(25) K. In addition, we have characterized the solid phases after crystallization of the two liquids and found that, while the high-density liquid transforms back to solid bP, the low-density liquid crystallizes into a more complex, partly crystalline and partly amorphous solid. The X-ray diffraction pattern of the crystalline component could be indexed as a mixture of red and violet P.

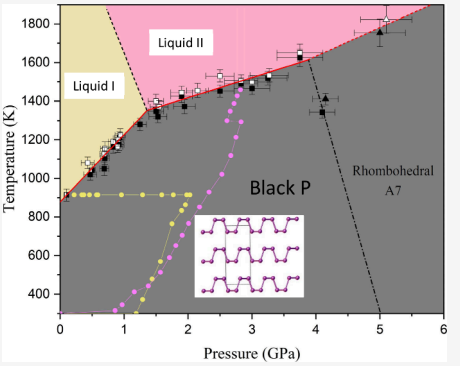

Phosphorus exhibits a very rich polymorphism under ambient[1] and nonambient pressure (P)-temperature (T) conditions.[2] The structure and physicochemical properties of the numerous allotropes of phosphorus have been extensively studied using a variety of experimental and computational methods.[2−14] Black phosphorus (bP), the densest allotrope at ambient conditions (2.69 g/cm^3),[1] was first obtained by subjecting white phosphorus (wP) to pressures above 1.2 GPa at 473 K.[15] It features a puckered layered structure with strong covalent intralayer bonds and weak van der Waals interlayer interactions, giving rise to largely anisotropic properties.[14,16,17] The ambient crystal structure has orthorhombic symmetry with space group *Cmca* and is often designated by its *Strukturbericht* symbol A17. A first-order phase transition to the A7 rhombohedral structure (space group $R\bar{3}m$) occurs at 5 GPa at 300 K. bP has been for a long time considered as the thermodynamically stable allotrope at ambient conditions, but some authors[18,19] have argued that either the triclinic red fibrous allotrope (rP) or the monoclinic Hittorf's violet phosphorus (vP), both composed of covalently linked tubular units, are more stable than bP. In contrast, recent calculations based on density-functional theory found that bP is slightly more stable than vP and rP.[20,21] The respective stability of these three polymorphs thus remains an active debate.

Upon heating at ambient pressure, bP does not melt but thermally decomposes above 685 K,[22,23] and the lowest P−T conditions at which melting of bP has been reported are 0.2 GPa and 991 K.[24] Another remarkable peculiarity that phosphorus only shares with sulfur[25] is that it exhibits a first-order phase transition in its stable liquid state[26] between a low-density liquid (LDL) supposedly composed of P_4 molecular units[26,27] and a high-density liquid (HDL) with a local atomic arrangement resembling that of bP.[27] The melting curve of bP has been investigated by several authors in the range 0.2−8 GPa using either electrical resistivity measurements[24,28] or in situ energy dispersive X-ray diffraction[28−30] in a piston−cylinder apparatus[31] or multianvil presses.[32] However, as shown in Figure 3, the measured melting curves differ greatly depending on the authors, particularly above 1 GPa: if some found a positive slope above this pressure,[24] others reported a negative one, resulting in a bell-shaped melting curve passing

Received: June 17, 2024
Revised: July 25, 2024
Accepted: July 31, 2024
Published: August 8, 2024

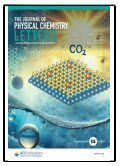

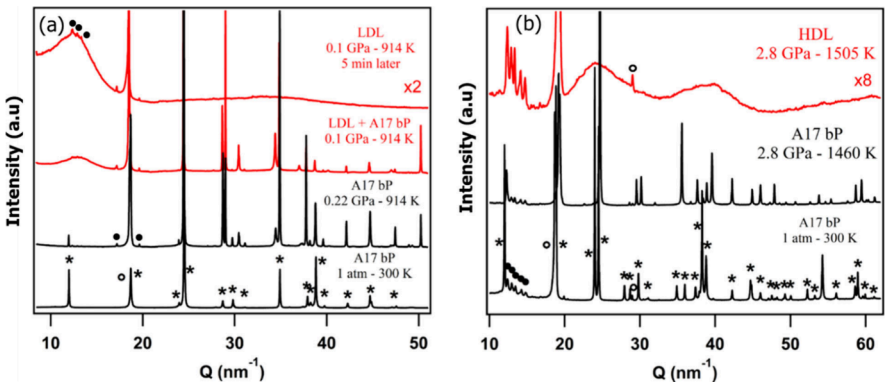

Figure 1. Melting criteria. XRD patterns of bP collected on decompression at constant temperature (914 K) toward the low-density liquid (a) and upon heating at constant pressure (2.8 GPa) toward the high-density liquid (b). The solid−liquid coexistence can be observed in the left panel (a). The black asterisks, black filled circles, and empty white circles indicate the Bragg reflections of bP, the boron-epoxy gasket, and the hexagonal boron nitride container, respectively.

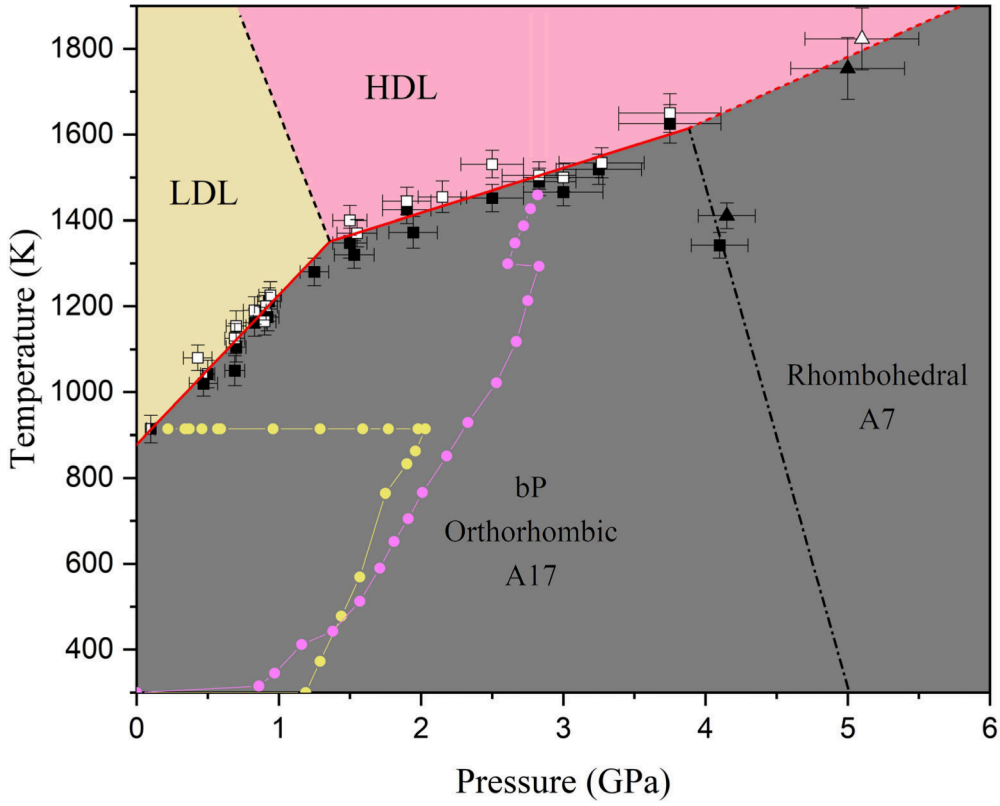

Figure 2. Melting curve of bP. Black and white filled symbols denote respectively the solid and liquid states. Squares and triangles indicate the A17 and A7 phases of solid bP, respectively. Two typical $P-T$ pathways followed in this work are highlighted (yellow and pink filled circles and lines).

through a maximum.[28−30] In addition, the melting curve of bP was found in some cases to exhibit an abrupt change of slope around 1 GPa,[28,30] supposedly as a result of the liquid−liquid transition, whereas others reported a continuous evolution.[24,29] There is thus at present no consensus on the location and shape of the melting line of bP below 5 GPa, nor on the existence of a triple point where the melting line intersects the liquid−liquid transition line.

Here, using an original P,T metrology,[33] we accurately determined the melting curve position and slope from 0.10(3) to 5.05(40) GPa and from 914(25) to 1788(70) K (numbers in parentheses give the estimated uncertainties) using in situ high-resolution synchrotron X-ray diffraction performed under high-pressure and -temperature conditions. Our results establish the existence of a solid-LDL-HDL triple point (SLHTP) located at 1.35(15) GPa and 1350(25) K. We have also observed that, unlike HDL, the LDL does not reversibly crystallize into bP below the SLHTP, but into a solid phase akin to crystalline red and violet P.

All experimental runs were carried out at the high-pressure X-ray diffraction beamline ID27 of the European Synchrotron Radiation Facility (Grenoble, France).[34] A VX5 Paris-Edinburgh press[35−37] served as pressure device. The sample consisted of a high purity (99.999+%) powder of black phosphorus (bP) produced as described in ref 38. It was confined in a diamond cylinder of 1 mm inner diameter and 1 mm height. The excellent thermal conductivity of diamond ensured very low temperature gradients within the X-ray

https://doi.org/10.1021/acs.jpclett.4c01794
J. Phys. Chem. Lett. 2024, 15, 8402−8409

probed volume. The diamond capsule was sealed using two chemically inert hexagonal boron nitride caps that also served as soft pressure medium. The high temperatures up to 1800 K were generated using a cylindrical graphite heater supplied with direct current. The graphite heater and diamond capsule were inserted in an X-ray transparent boron-epoxy gasket that served as thermal and electrical insulator.[37] In situ monochromatic X-ray diffraction (XRD) experiments have been conducted in transmission geometry either at 20.0 keV (λ = 0.6199 Å) or at 33.169 keV (λ = 0.3738 Å). Two-dimensional diffraction patterns have been collected using either a MAR165 CCD detector from MAR Research or an EIGER2 9 M photon counting system from DECTRIS. A multichannel collimator (MCC) was used to remove most of the parasitic elastic and inelastic X-ray signal coming from the sample environment.[39] The sample to detector distance, detector tilt angles and X-ray beam center were calibrated using a LaB_6 powder from the National Institute of Standards and Technology (NIST). The two-dimensional XRD images were integrated using the PyFAI code[40] as implemented in DIOPTAS.[41] XRD patterns were analyzed using GSAS[42] or FULLPROF.2k.[43]

The main objective of this study being to establish the position and shape of the melting curve of bP, it is of crucial importance to accurately determine the pressure and temperature at which the XRD measurements have been performed. Here, we have employed an original *P*,*T* metrology that is detailed in ref 33. This method exploits the fact that bP is quasi-incompressible along the *a* crystallographic axis and exhibits a small but finite thermal expansion coefficient in the same direction (α_a= 6.46(6) × 10^{-6} K^{-1}). This is used to simultaneously determine *P* and *T* from the XRD patterns of bP. In practice, the *a* lattice parameter of bP is determined from the (h00) type Bragg reflections, then the temperature is derived using the following relation:

$$T/\mathrm{K} = \frac{a/a_0 - 1}{6.46 \times 10^{-6}} + 300$$

where a_0 is the value of *a* at ambient conditions. The pressure is then obtained from the measured volume of bP corrected by the thermal expansion effect, using the third-order Birch−Murnaghan equation of state and thermal coefficients reported in ref 33. This method enables the determination of *P* and *T* with an accuracy of ±25 K and 0.1 GPa in the entire *P*,*T* stability field of bP up to 5 GPa and 1700 K.

Another critical aspect regarding melting studies resides in the use of an unambiguous melting criterion. Here we have employed a standard and well-established criterion:[44−46] the X-ray signature associated with the loss of crystalline order that occurs at melting. As shown in Figure 1, high quality diffraction patterns were obtained for solid and liquid phosphorus. The transition between these two states is evidenced by the disappearance of the Bragg reflections of bP and the concomitant appearance of a strong liquid diffuse X-ray signal when the melting line is crossed.

Typical *P*,*T* pathways in the phase diagram of bP in the ranges 0.1−5.3 GPa and 300−1800 K are shown in Figure 2. A freshly loaded sample was used for each of them. XRD patterns were systematically collected along 19 distinct *P*,*T* pathways leading to the determination of the same number of melting points. It is worth nothing that we were able to collect data points at very low pressure down to 0.10 ± 0.03 GPa, which is challenging due to the mechanical instability of bP near ambient pressure.[22,23] In practice, to reach the melting curve, the temperature was increased by small increments of approximately 30 K at constant pressure or the pressure was finely reduced at constant temperature by steps of 0.1 GPa to bracket the melting pressures and temperatures with an accuracy of ±25 K and 0.1 GPa. At pressures below 1.2 GPa, the melting of bP toward the LDL has been clearly assessed by the appearance of a strong diffuse X-ray signal which exhibits an intense first sharp diffraction peak (FSDP) at a Q value of 13 nm^{-1} (Figure 1a). At higher pressures (P > 1.2 GPa), the diffracted signal I(Q) of the melt exhibits two distinct maxima at 23 and 40 nm^{-1} (Figure 1b) that are unambiguous signatures of the HDL.[27] It is worth noting that the remaining Bragg reflections occurring at low Q (Q < 30 nm^{-1}) arise from the sample container components (boron-epoxy gasket, graphite heater and h-BN capsule) that are not entirely filtered out by the MCC.[39]

In agreement with previous works,[24,28−30] we did not observe any structural phase transition prior to the melting of the A17 phase of phosphorus, demonstrating that solid bP directly melts into either the LDL or HDL. We could also clearly observe the coexistence between solid bp and the LDL at 0.10(3) GPa and 914(25) K, as illustrated in Figure 1a, and at 0.50(5) GPa and 1042(25) K. These are strong arguments in favor of A17 bP being the thermodynamically stable allotrope of phosphorus in the 0.1−5 GPa range at all temperatures below the melting line. As mentioned above, A17 bP transforms at higher pressure to the A7 rhombohedral phase ($R\bar{3}m$ space group).[2] In the course of this experiment, we could determine one melting point in the stability field of the A7 polymorph at 5.05 GPa and 1780 K. From this information and the location of 2 additional points on the A17 to A7 solid−solid transition line at 4.12 GPa and 1375 K (this work) and at 5 GPa and 300 K,[2] we could infer the position of the A17-A7-HDL triple point at 3.88 ± 0.15 GPa and 1615 ± 25 K. We also note that there seems to be a slight increase in the slope of the melting curve above this triple point, but since this is constrained by a single melting point, additional measurements are required to confirm this.

The melting curve of bP and the *P*,*T* location of the individual melting points are presented in Figure 2 and Table 1, respectively. Within present uncertainties, the melting temperature increases linearly with pressure and exhibits two distinct pressure regimes. Indeed, the slope of the melting curve is suddenly and significantly modified at the SLHTP: its value is reduced by a factor of ∼3.3 varying from 348 ± 21 to 105 ± 12 K·GPa^{-1}. This abrupt change is undoubtedly related

Table 1. Measured Melting Points of A17 bP, except for the Points Indicated by * Which Corresponds to the Melting of the A7 Solid

Pressure (GPa)	Temp (K)	Pressure (GPa)	Temp (K)
0.10 (3)	914 (25)	1.54 (12)	1355 (30)
0.45 (10)	1050 (25)	1.90 (15)	1435 (30)
0.50 (5)	1042 (25)	2.05 (15)	1414 (35)
0.69 (7)	1088 (30)	2.50 (20)	1492 (30)
0.70 (7)	1129 (30)	2.83 (25)	1498 (30)
0.83 (8)	1176 (30)	3.00 (28)	1483 (30)
0.92 (8)	1205 (30)	3.26 (30)	1527 (35)
0.93 (8)	1200 (30)	3.75 (35)	1637 (45)
1.25 (10)	1330 (30)	5.05 (40)*	1788 (70)*
1.50 (12)	1374 (30)		

https://doi.org/10.1021/acs.jpclett.4c01794
J. Phys. Chem. Lett. 2024, 15, 8402−8409

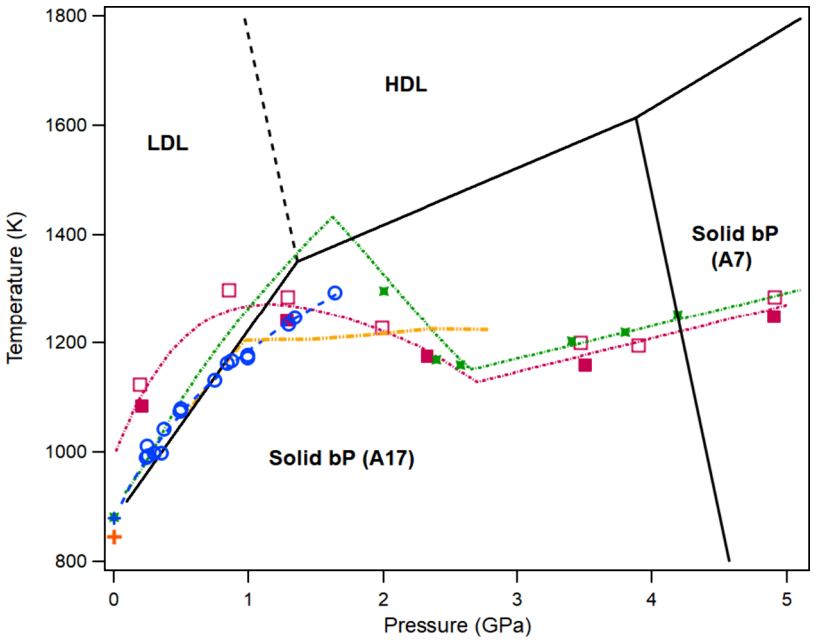

Figure 3. Comparison between the melting curve of bP from this work (black line) and the melting curves reported by Akahama et al.[29] (red dashed line and symbols), Marani and Guarise[24] (blue dashed line and symbols), Mizutani et al.[30] (yellow dashed line), and Solozhenko and Turkevich[28] (green dashed line and symbols). Plain and empty squares denote respectively the solid and liquid states. The colored crosses indicate the melting temperatures obtained by extrapolation of the melting curves to ambient pressure. The dashed line is the liquid−liquid transition line between LDL and HDL inferred in the present work as explained in the text.

to the liquid−liquid transition and the large density difference between the LDL and HDL reported in refs 26 and 47. Indeed, from the Clausius−Clapeyron relation,[48,49] significant differences in the melting volume and entropy between the low- and high-pressure regimes should translate into a strong change of the melting slope. Unlike some literature reports,[28,29] we find here that the slope of the melting line remains positive above the SLHTP, meaning that solid bP is always denser than the liquid. The SLHTP was located at the intersection of the low- and high-pressure melting lines at 1.35 ± 0.15 GPa and 1350 ± 25 K. We note that these $P-T$ coordinates of the SLHTP slightly differ from those that can be inferred from the intersection of the liquid−liquid transition (LLT) line reported in ref 50 and the present melting line, which is likely due to the difference in $P-T$ metrology used in the two studies. In Figure 2, the LLT line was therefore constructed using the presently determined position of the SLHTP, and the slope of the LLT line reported by Monaco et al.[50]

At our lowest investigated pressure of 0.1 GPa, bP melts at 914 K. Extropolating our melting line below the SLHTP, we estimate the ambient pressure melting point to be at 880 ± 15 K, in fair agreement with the extrapolations reported earlier.[24,29,30] A comparison of the bP melting curve determined in this study with literature data is presented in Figure 3. As recalled in the introduction, the literature melting data of bP show significant disagreements, notably above 1 GPa, which is probably due to a variety of experimental problems as discussed in the following. The melting data of Marani and Guarise[24] were determined using the change in sample resistivity upon melting as a criterion. They agree fairly well with ours up to ∼1 GPa but indicates lower melting temperatures at higher pressures and do not exhibit a sudden break in slope up to their maximum pressure of 1.6 GPa. The melting points in ref 28, also mostly derived from the resistivity change at melting, start above 2 GPa and suggest a negative melting slope above the SLHTP. The slope becomes positive again above the A17-A7-HDL triple point, the latter being located at much lower $P-T$ conditions (around 2.5 GPa and 1150 K) than estimated in the present work. The other two reported melting studies[29,30] were carried out using the same in situ energy dispersive X-ray (EDX) diffraction methodology in a multianvil press,[32] but do not agree with each other. Akahama et al.[29] reported a maximum of the melting curve around 1 GPa, followed by a reduction of the melting temperature toward the A17-A7-HDL triple point located around 2.7 GPa and 1100 K; while Mizutani et al.[30] observed a positive slope of the melting line up to about 3 GPa, and a sudden change of slope around 1 GPa. The latter agrees reasonably well with our results, except that the slope of the melting line beyond the SLHTP (15 K·GPa^{-1}) differs from that found here (105 ± 12 K·GPa^{-1}) by an order of magnitude. The discrepancies between these previous works and with present results could have several origins. First, in all these studies, the authors used a thermocouple to determine the temperature and neglected the pressure effect on its response, which however has been shown to be significant.[51] A second possible source of error comes from the pressure and temperature gradient between the calibrant and the sample: in multianvil press experiments,[32] the pressure calibrant and the temperature probe is always located at a finite distance (typically 1 mm) from the sample, which inevitably results in systematic errors in P and T. As explained above, here we used the bP powder sample itself as the P,T sensor, which eliminates this problem. Third, the melting criterion in ref 28 was solely based on the disappearance of the Bragg peaks of the solid. It is well established[52,53] that strong recrystallization effects occur at temperatures lower than melting, which transforms the large number of randomly oriented crystallites into fewer and larger crystals, and as a consequence, converts the Debye−Scherrer rings into a few diffraction spots. Since in the EDX method the

https://doi.org/10.1021/acs.jpclett.4c01794
J. Phys. Chem. Lett. 2024, 15, 8402−8409

diffracted X-rays are collected using a single-point detector[54] that covers only a very small fraction of the reciprocal space, melting can be confused with recrystallization.

In addition to the determination of the melting curve of bP, we have studied the reversibility of the phase transition by in situ characterization of the crystal structure of the solids recovered after temperature quenching. On quenching the HDL from $P-T$ conditions beyond the SLHTP, the bP phase is recovered, in agreement with previous reports.[29,55] By contrast, starting from the LDL at P,T conditions lower than those of the SLHTP, the solid phase recovered at ambient conditions displays an XRD pattern which is different and much more complex than that of bP. As an illustration, panels a and b of Figure 4 show the XRD image and pattern of a sample that was melted at 0.5 GPa, slowly cooled to room temperature keeping the force constant, and then decompressed to ambient P. This pattern is composed of Bragg peaks on top of a slowly oscillating background, suggesting that the sample is partly crystalline and partly amorphous. The Bragg peaks cannot be indexed by the known crystalline forms of fibrous red phosphorus[56] nor Hittorf's violet phosphorus,[57] but a reasonable Le Bail refinement could be obtained using a mixture of red and violet P, as shown in Figure 4b. We recall that the structures of these two phosphorus allotropes are composed of the same tubular units and only differ by the arrangement of the latter (parallel vs orthogonal sets in the triclinic red and monoclinic violet P, respectively). Moreover DFT calculations indicate that the two polymorphs have the same cohesive energies.[20,21,58] Unfortunately, the large texture of the quenched solid, clearly apparent in the two-dimensional XRD image (Figure 4), prevents from performing any further structural (Rietveld type) refinement. We thus cannot exclude that the recovered crystal is another, yet unreported crystalline form of phosphorus. We also note that Akahama et al.[29] briefly reported a similar observation for a sample recovered from the liquid melted at 0.29 GPa, whose XRD pattern could not be indexed with a known crystalline form. Unfortunately, this pattern was not provided in the report, so comparison with our results cannot be made.

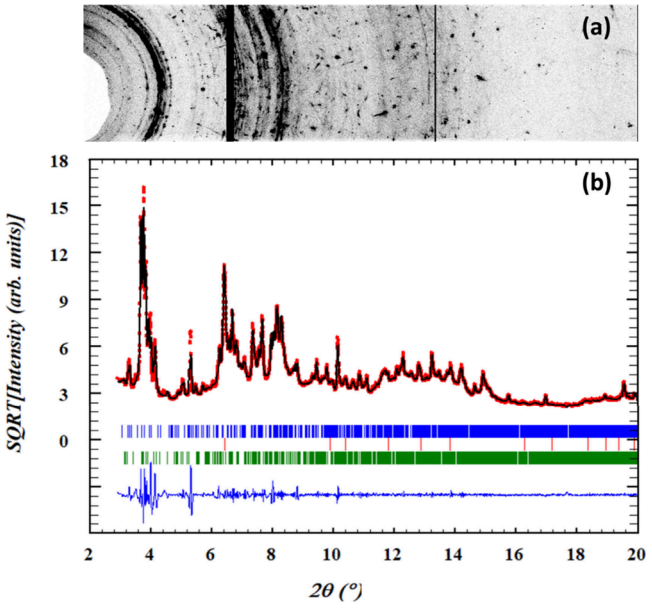

Figure 4. 2D XRD image (a) and integrated pattern (b) of the sample that crystallized upon cooling the LDL at 0.50(5) GPa and was decompressed to ambient conditions. The X-ray wavelength was 0.3738 Å. The *y*-scale in panel b is the square root of the measured intensity to emphasize the oscillations of the background that likely comes from an amorphous part of the sample. The red dots are the measured data, and the black line is a Le Bail fit of the pattern using 3 phases: fibrous red P[56] (blue ticks), violet P[57] (green ticks), and hBN (red ticks). In the fit, the lattice parameters for red and violet P were kept fixed at their reference values to prevent convergence to unrealistic ones due to the strong peak overlap. Only one peak profile parameter and a global zero offset were refined. The background was represented by linear sections between 35 points and was not refined. The bottom blue line is the difference between the data and the Le Bail fit.

The reversibility of melting above the SLHTP suggests a similarity of the local atomic order of the HDL and bP, as also suggested by computer simulations.[27] On the contrary, its irreversibility below the SLHTP indicates that the atomic arrangement of the LDL strongly differs from that of bP. Indeed, in such case one may expect a large surface energy between LDL and bP, which makes the nucleation of bP unfavored compared to other allotropes. A similar case has been reported in H_2O:[59] when the liquid is rapidly overcompressed to 1.7 GPa, it crystallizes into the metastable ice VII rather than the stable ice VI. This is due to a smaller liquid/ice VII surface energy at high P compared to that of the liquid/ice VI, itself resulting from the fact that the local structure of the dense liquid is closer to that of ice VII[60,61]. A more detailed study of the quenched solid and of its melting line is needed to better understand the irreversible character of the melting of bP below the triple point, and will be the subject of future works. The different nature of the quenched phases from LDL and HDL indirectly confirms that the local atomic arrangement in these two liquid phases is substantially different.

In conclusion, we employed in situ high-resolution X-ray diffraction to accurately determine the melting curve of bP in an extended P,T range up to 5 GPa and 1700 K, and investigate the reversibility of the melting transition. We used the disappearance of the solid Bragg peaks and concomitant appearance of the liquid diffuse scattering as an unambiguous criterion of melting. Pressure and temperature was determined from the bP sample itself up to the melting point, which ensured the absence of systematic errors due to pressure or temperature gradients. To our knowledge, we have observed here for the first time the coexistence of bP and the liquid phase at melting, providing strong support that bP is the thermodynamically stable phase up to the melting temperature in the 0.1−5 GPa range. The measured 19 melting points enabled to identify two distinct regimes of melting, in correspondence with the $P-T$ ranges of stability of the low- and high- density liquids. In both cases, the melting temperature increases linearly with pressure but the slope of the melting line is reduced by a factor ∼3 in the HDL domain. The sudden break of slope unambiguously establishes a triple point between the LDL, HDL and crystalline A17 bP in the P,T phase diagram of P. The contrasting slope of the melting curve confirms the important density difference between LDL and HDL. Unlike some previous reports, however, we find that the slope of the melting line is always positive, meaning that solid bP is always denser than its liquid. The observation that the low-density liquid does not crystallize into bP unlike HDL, but into a more complex solid composed of a mixture of red and violet phosphorus and, an amorphous component suggests

https://doi.org/10.1021/acs.jpclett.4c01794
J. Phys. Chem. Lett. 2024, 15, 8402−8409

that the short-range order in the LDL, currently considered as composed of P_4 molecular units, could be more complex. This should stimulate further structural studies of the LDL and of the transition line between the LDL and HDL.

■ ASSOCIATED CONTENT

Supporting Information

The Supporting Information is available free of charge at https://pubs.acs.org/doi/10.1021/acs.jpclett.4c01794.

Transparent Peer Review report available (PDF)

■ AUTHOR INFORMATION

Corresponding Authors

Mohamed Mezouar − *European Synchrotron Radiation Facility (ESRF), 38043 Grenoble, France;* orcid.org/0000-0001-5336-544X; Phone: +33 (0)4 76 88 25 15; Email: mezouar@esrf.fr

Frédéric Datchi − *Institut de Minéralogie, de Physique des Milieux Condensés et de Cosmochimie (IMPMC), Sorbonne Université, CNRS UMR 7590, MNHN, F-75005 Paris, France;* orcid.org/0000-0003-1252-1770; Phone: +33(0)1 44 27 45 06; Email: frederic.datchi@sorbonne-universite.fr

Authors

Hermann Muhammad − *European Synchrotron Radiation Facility (ESRF), 38043 Grenoble, France*

Gaston Garbarino − *European Synchrotron Radiation Facility (ESRF), 38043 Grenoble, France*

Laura Henry − *Synchrotron SOLEIL, 91192 Gif-sur-Yvette, France*

Tomasz Poręba − *European Synchrotron Radiation Facility (ESRF), 38043 Grenoble, France; Laboratory for Quantum Magnetism, Ecole Polytechnique Fédérale Lausanne, CH-1015 Lausanne, Switzerland;* orcid.org/0000-0002-0383-4639

Max Gerin − *European Synchrotron Radiation Facility (ESRF), 38043 Grenoble, France;* orcid.org/0009-0000-1338-2667

Matteo Ceppatelli − *LENS, European Laboratory for Nonlinear Spectroscopy, I-50019 Firenze, Italy; ICCOM-CNR, Institute of Chemistry of OrganoMetallic Compounds, National Research Council of Italy Via Madonna del Piano 10, I-50019 Firenze, Italy;* orcid.org/0000-0002-0688-5167

Manuel Serrano-Ruiz − *ICCOM-CNR, Institute of Chemistry of OrganoMetallic Compounds, National Research Council of Italy Via Madonna del Piano 10, I-50019 Firenze, Italy;* orcid.org/0000-0002-6372-3586

Maurizio Peruzzini − *ICCOM-CNR, Institute of Chemistry of OrganoMetallic Compounds, National Research Council of Italy Via Madonna del Piano 10, I-50019 Firenze, Italy;* orcid.org/0000-0002-2708-3964

Complete contact information is available at: https://pubs.acs.org/10.1021/acs.jpclett.4c01794

Author Contributions

The original idea was defined by M.M. and F.D. Experiments were performed by H.M., L.H., G.G., M.G., T.P., M.C., M.S.D., F.D., and M.M. with equal contributions. The data were analyzed and the figures were produced by H.M. The manuscript was written by H.M., M.M., and F.D. All authors have given approval to the final version of the manuscript.

Notes

The authors declare no competing financial interest.

■ ACKNOWLEDGMENTS

Thanks are expressed to EC through the European Research Council (ERC) for funding the project PHOSFUN "Phosphorene functionalization: a new platform for advanced multifunctional materials" (Grant Agreement No. 670173) through an ERC Advanced Grant, and the Agence Nationale de la Recherche (ANR) for financial support under Grant ANR-21-CE30-0032-01 (LILI). We acknowledge the ESRF for the provision of beam time on the High-Pressure Beamline ID27. Thanks are expressed also to the projects "GreenPhos−alta pressione" (CNR), HP-PHOTOCHEM (Fondazione Cassa di Risparmio di Firenze), and PRIN 2017 KFY7XF FERMAT "FastElectRon dynamics in novel hybrid-2D MATerials" (MUR).

■ REFERENCES

(1) Corbridge, D. E. C. *Phosphorus: Chemistry, Biochemistry and Technology*, 6th ed.; Taylor & Francis: New York, 2013. DOI: 10.1201/b12961.

(2) Scelta, D.; Baldassarre, A.; Serrano-Ruiz, M.; Dziubek, K.; Cairns, A. B.; Peruzzini, M.; Bini, R.; Ceppatelli, M. The p-sc structure in phosphorus: bringing order to the high pressure phases of group 15 elements. *Chem. Commun.* **2018**, *54*, 10554−10557.

(3) Corbridge, D.; Lowe, E. Structure of white phosphorus: Single crystal X-ray examination. *Nature* **1952**, *170*, 629.

(4) Simon, A.; Borrmann, H.; Craubner, H. Crystal structure of ordered white phosphorus (β-P). *Sulfur Relat. Elem.* **1987**, *30* (1−2), 507−510.

(5) Okudera, H.; Dinnebier, R. E.; Simon, A. The crystal structure of γ-P4, a low temperature modification of white phosphorus. *Z. Kristallogr.* **2005**, *220*, 259−264.

(6) Shanabrook, B. V.; Lannin, J. S. Structural and vibrational properties of amorphous phosphorus. *Phys. Rev. B* **1981**, *24*, 4771−4780.

(7) Elliott, S.; Dore, J.; Marseglia, E. The structure of amorphous phosphorus. *J. Phys. Colloques* **1985**, *46*, C8-349−C8-353.

(8) Jóvári, P.; Pusztai, L. On the structure of amorphous red phosphorus. *Appl. Phys. A: Mater. Sci. Process.* **2002**, *74*, s1092−s1094.

(9) Zaug, J. M.; Soper, A. K.; Clark, S. M. Pressure-dependent structures of amorphous red phosphorus and the origin of the first sharp diffraction peaks. *Nat. Mater.* **2008**, *7*, 890−899.

(10) Rissi, E. N.; Soignard, E.; McKiernan, K. A.; Benmore, C. J.; Yarger, J. L. Pressure-induced crystallization of amorphous red phosphorus. *Solid State Commun.* **2012**, *152*, 390−394.

(11) Zhou, Y.; Kirkpatrick, W.; Deringer, V. L. Cluster fragments in amorphous phosphorus and their evolution under pressure. *Adv. Mater.* **2022**, *34*, 2107515.

(12) Jamieson, J. C. Crystal structures adopted by black phosphorus at high pressures. *Science* **1963**, *139*, 1291−1292.

(13) Crichton, W.; Mezouar, M.; Monaco, G. *Phosphorus: New in situ powder data from large-volume apparatus*. Cambridge University Press, 2003; Vol. *18*, pp 155−158.

(14) Scelta, D.; Baldassarre, A.; Serrano-Ruiz, M.; Dziubek, K.; Cairns, A. B.; Peruzzini, M.; Bini, R.; Ceppatelli, M. Interlayer bond formation in black phosphorus at high pressure. Angew. *Chem. Int. Ed.* **2017**, *56*, 14135−14140.

(15) Bridgman, P. W. Two new modifications of phosphorus. *J. Am. Chem. Soc.* **1914**, *36* (7), 1344−1363.

(16) Hultgren, R.; Gingrich, N. S.; Warren, B. E. The atomic distribution in red and black phosphorus and the crystal structure of black phosphorus. *J. Chem. Phys.* **1935**, *3*, 351−355.

(17) Brown, A.; Rundqvist, S. Refinement of the crystal structure of black phosphorus. *Acta Crystallogr.* **1965**, *19*, 684−685.
(18) Brazhkin, V. V.; Zerr, A. J. Relative stability of red and black phosphorus at P < I GPa. *J. Mater. Sci.* **1992**, *27*, 2677−2681.
(19) Zhang, L.; Huang, H.; Zhang, B.; Gu, M.; Zhao, D.; Zhao, X.; Li, L.; Zhou, J.; Wu, K.; Cheng, Y.; Zhang, J. Structure and Properties of Violet Phosphorus and Its Phosphorene Exfoliation. *Angew. Chem., Int. Ed.* **2020**, *59*, 1074.
(20) Bachhuber, F.; von Appen, J.; Dronskowski, R.; Schmidt, P.; Nilges, T.; Pfitzner, A.; Weihrich, R. The extended stability range of phosphorus allotropes. *Angew. Chem., Int. Ed.* **2014**, *53*, 11629.
(21) Zhou, Y.; Elliott, S. R.; Deringer, V. L. Structure and Bonding in Amorphous Red Phosphorus. *Angew. Chem., Int. Ed.* **2023**, *62*, No. e202216658.
(22) Luo, W.; Yang, R.; Liu, J.; Zhao, Y.; Zhu, W.; Xia, G. M. Thermal sublimation: a scalable and controllable thinning method for the fabrication of few-layer black phosphorus. *Nanotechnology* **2017**, *28*, 285301.
(23) Henry, L.; Svitlyk, V.; Mezouar, M.; Sifre, D.; Garbarino, G.; Ceppatelli, M.; Serrano-Ruiz, M.; Peruzzini, M.; Datchi, F. Anisotropic thermal expansion of black phosphorus from nanoscale dynamics of Phosphorene layers. *Nanoscale* **2020**, *12*, 4491−4497.
(24) Marani, A.; Guarise, G. B. Fusione del fosforo nero fino a 16.000 atm. *Chim. Ind.* **1968**, *50*, 663−665.
(25) Henry, L.; Mezouar, M.; Garbarino, G.; Sifré, D.; Weck, G.; Datchi, F. Liquid-liquid transition and critical point in sulfur. *Nature* **2020**, *584*, 382−386.
(26) Katayama, Y.; Mizutani, T.; Utsumi, W.; Shimomura, O.; Yamakata, M.; Funakoshi, K. A first-order liquid-liquid phase transition in phosphorus. *Nature* **2000**, *403*, 170−173.
(27) Senda, Y.; Shimojo, F.; Hoshino, K. The metal-nonmetal transition of liquid phosphorus by *ab initio* molecular dynamics simulations. *J. Phys.: Condens. Matter* **2002**, *14*, 3715−3723.
(28) Solozhenko, V. L.; Turkevich, V. P-T. phase diagram of phosphorus revisited. *J. Phys. Chem. C* **2023**, *127* (12), 6088−6092.
(29) Akahama, Y.; Utsumi, W.; Endo, S.; Kikegawa, T.; Iwasaki, H.; Shimomura, O.; Yagi, T.; Akimoto, S. Melting curve of black phosphorus. *Phys. Lett. A* **1987**, *122*, 129−131.
(30) Mizutani, T.; Katayama, Y.; Utsumi, W.; Funakoshi, K.; Yamakata, M.; Shimomura, O. Anomaly in the melting curve of black phosphorus associated with a liquid-liquid transition. *Science Technol. High Press* **2000**, *1*, 525−528. *(Proceedings of AIRAPT-17)*
(31) Bridgman, P. W. The technique of high pressure experimenting. *Proc. Am. Acad. Arts Sci.* **1914**, *49* (11), 627−643.
(32) Kawai, N.; Togaya, M.; Onodera, A. A new device for pressure vessels. *Proc. Jpn. Acad.* **1973**, *49* (8), 623−626.
(33) Muhammad, H.; Mezouar, M.; Garbarino, G.; Poręba, T.; Confalonieri, G.; Ceppatelli, M.; Serrano-Ruiz, M.; Peruzzini, M.; Datchi, F. Anisotropic thermo-mechanical response of layered hexagonal boron nitride and black phosphorus: application as a simultaneous pressure and temperature sensor. *Nanoscale* **2024**, *16*, 9096−9107.
(34) Poręba, T.; Comboni, D.; Mezouar, M.; Garbarino, G.; Hanfland, M. Tracking structural phase transitions via single crystal x-ray diffraction at extreme conditions: advantage of extremely brilliant source. *J. Phys.: Condens. Matter* **2023**, *35*, 054001.
(35) Besson, J. M.; Hamel, G.; Grima, P.; Nelmes, R. J.; Loveday, J. S.; Hull, S.; Häusermann, D. A large volume pressure cell for high temperatures. *High Press. Res.* **1992**, *8*, 625.
(36) Klotz, S.; Strassle, T.; Rousse, G.; Hamel, G.; Pomjakushin, V. Angle-dispersive neutron diffraction under high pressure to 10 GPa. *Appl. Phys. Lett.* **2005**, *86*, 031917.
(37) Morard, G.; Mezouar, M.; Rey, N.; Poloni, R.; Merlen, A.; Le Floch, S.; Toulemonde, P.; Pascarelli, S.; San Miguel, A.; Sanloup, C.; Fiquet, G. Optimization of Paris-Edinburgh press cell assemblies for *in situ* monochromatic X-ray diffraction and X-ray absorption. *High Press. Res.* **2007**, *27*, 223.
(38) Serrano-Ruiz, M.; Caporali, M.; Ienco, A.; Piazza, V.; Heun, S.; Peruzzini, M. The role of water in the preparation and stabilization of high-quality phosphorene flakes. *Adv. Mater. Interfaces* **2016**, *3*, 1500441.
(39) Mezouar, M.; Faure, P.; Crichton, W.; Rambert, N.; Sitaud, B.; Bauchau, S.; Blattmann, G. Multichannel collimator for structural investigation of liquids and amorphous materials at high pressures and temperatures. *Rev. Sci. Instrum.* **2002**, *73*, 3570−3574.
(40) Ashiotis, G.; Deschildre, A.; Nawaz, Z.; Wright, J. P.; Karkoulis, D.; Picca, F. E.; Kieffer, J. The fast azimuthal integration Python library: pyFAI. *J. Appl. Crystallogr.* **2015**, *48*, 510−519.
(41) Prescher, C.; Prakapenka, V. B. DIOPTAS: A program for reduction of two-dimensional X-ray diffraction data and data exploration. *High. Press. Res.* **2015**, *35*, 223−230.
(42) Toby, B. H. EXPGUI, a graphical user interface for GSAS. *J. Appl. Crystallogr.* **2001**, *34*, 210−213.
(43) Rodriguez-Carvajal, J. Recent advances in magnetic structure determination by neutron powder diffraction + FullProf. *Physica B* **1993**, *192*, 55.
(44) Queyroux, J.-A.; Ninet, S.; Weck, G.; Garbarino, G.; Plisson, T.; Mezouar, M.; Datchi, F. Melting curve and chemical stability of ammonia at high pressure: a combined X-ray diffraction and Raman study. *Phys. Rev. B* **2019**, *99*, 134107.
(45) Dewaele, A.; Mezouar, M.; Guignot, N.; Loubeyre, P. Melting of lead under high pressure studied using second-scale time-resolved X-ray diffraction. *Phys. Rev. B* **2007**, *76*, 144106.
(46) Anzellini, S.; Alfé, D.; Pozzo, M.; Errandonea, D. Melting line of calcium characterized by in situ LH-DAC XRD and first-principles calculations. *Sci. Rep.* **2021**, *11*, 15025.
(47) Katayama, Y.; Inamura, Y.; Mizutani, T.; Yamakata, M.; Utsumi, W.; Shimomura, O. Macroscopic separation of dense fluid phase and liquid phase of phosphorus. *Science* **2004**, *306*, 848−851.
(48) Clausius, R. Ueber die bewegende Kraft der Wärme und die Gesetze, welche sich daraus für die Wärmelehre selbst ableiten lassen. *Annalen der Physik* **1850**, *155*, 368−397.
(49) Clapeyron, M. C. Mémoire sur la puissance motrice de la chaleur. *J. École Polytech.* **1834**, No. 23, 153−190.
(50) Monaco, G.; Falconi, S.; Crichton, W. A.; Mezouar, M. Nature of the First-Order Phase Transition in Fluid Phosphorus at High Temperature and Pressure. *Phys. Rev. Lett.* **2003**, *90*, 255701.
(51) Kennedy, G. C.; Newton, R. C. The effect of pressure on the electromotive force of a platinum-bismuth thermocouple. *J. Geophys. Res.* **1961**, *66*, 1491−1493.
(52) Anzellini, S.; Dewaele, A.; Mezouar, M.; Loubeyre, P.; Morard, G. Melting or iron at Earth's inner core boundary based on X-ray diffraction. *Science* **2013**, *340*, 464−466.
(53) Dewaele, A.; Mezouar, M.; Guignot, N.; Loubeyre, P. High Melting Points of Tantalum in a Laser-Heated Diamond Anvil Cell. *Phys. Rev. Lett.* **2010**, *104*, 255701.
(54) Dicken, A. J.; Evans, J. P. O.; Rogers, K. D.; Greenwood, C.; Godber, S. X.; Prokopiou, D.; Stone, N.; Clement, J. G.; Lyburn, I.; Martin, R. M.; Zioupos, P. Energy-dispersive X-ray diffraction using an annular beam. *Opt. Express* **2015**, *23*, 13443−13454.
(55) Endo, S.; Akahama, Y.; Terada, S.; Narita, S. Growth of large single crystals of black phosphorus under high pressure. *Jpn. J. Appl. Phys.* **1982**, *21*, L482.
(56) Ruck, M.; Hoppe, D.; Wahl, B.; Simon, P.; Wang, Y.; Seifert, G. Fibrous red phosphorus. *Angew. Chem., Int. Ed.* **2005**, *44*, 7616−7619.
(57) Wang, Y.; Jin, M.; Gu, M.; Zhao, X.; Xie, J.; Meng, G.; Cheng, Y.; He, J.; Zhang, J. Synthesis of violet phosphorus with large lateral sizes to facilitate nano-device fabrications. *Nanoscale* **2023**, *15*, 12406.
(58) Deringer, V. L.; Caro, M. A.; Csányi, G. A general-purpose machine-learning force field for bulk and nanostructured phosphorus. *Nat. Commun.* **2020**, *11*, 5461.
(59) Lee, G. W.; Evans, W. J.; Yoo, C.-S. Crystallization of water in a dynamic diamond-anvil cell: Evidence for ice VII-like local order in supercompressed water. *Phys. Rev. B* **2006**, *74*, 134112.
(60) Soper, A. K.; Ricci, M. A. Structures of high-density and low density water. *Phys. Rev. Lett.* **2000**, *84*, 2881.

https://doi.org/10.1021/acs.jpclett.4c01794
J. Phys. Chem. Lett. 2024, 15, 8402−8409

(61) Saitta, A. M.; Datchi, F. Structure and phase diagram of high-density water: The role of interstitial molecules. *Phys. Rev. E* **2003**, *67*, 020201.

https://doi.org/10.1021/acs.jpclett.4c01794
J. Phys. Chem. Lett. 2024, 15, 8402−8409